行政院國家科學委員會專題研究計畫 成果報告

熱機處理程序對含鈧鎂鋰合金性質與成形性的影響研究
研究成果報告(精簡版)

計 畫 類 別 ：個別型
計 畫 編 號 ：NSC 97-2221-E-216-010-
執 行 期 間 ：97 年 08 月 01 日至 98 年 07 月 31 日
執 行 單 位 ：中華大學機械與航太工程研究所

計 畫 主 持 人：吳泓瑜

計畫參與人員：碩士班研究生-兼任助理人員：徐維謙
碩士班研究生-兼任助理人員：蔡欣翰
碩士班研究生-兼任助理人員：黃志超

報 告 附 件 ：出席國際會議研究心得報告及發表論文

處 理 方 式 ：本計畫可公開查詢

中 華 民 國 98 年 10 月 13 日

行政院國家科學委員會專題研究計畫成果報告

熱機處理程序對含抗鎂鋰合金性質與成形性的影響研究

Effects of thermomechanical treatments on the properties and formability of an Mg-Li alloy containing Sc

計畫編號：NSC 97-2221-E-216-010

執行期間：97年 8月 1日至98年 7月31日

計劃主持人: 吳泓瑜　　中華大學機械與航太工程研究所教授

E-mail: ncuwu@chu.edu.tw

計畫參與人員：徐維謙、蔡欣翰、黃志超 中華大學機械工程研究所研究生

中文摘要

本研究以含10wt%鋰的鎂鋰合金為基材，主要以添加Al、Zn及微量的Sc元素等來改善Mg-Li 合金之機械性質，並研究鈧對鎂鋰鋁鋅合金之影響。實驗設計包括熱處理、冷作加工、成形性參數量測、成形性實驗等，探討熱機處理程序對含鈧鎂鋰合金機械性質、應變硬化及成形極限的影響。實驗結果顯示，含Sc鎂鋰合金具有應變硬化的硬化效果，且退火熱處理，有助於提升加工硬化的效果。Kocks-Mecking法的分析顯示，含鈧鎂鋰合金具有第三及第四階段(Stage III and IV)的應變硬化率特性。成形性測試結果顯示，軋延方向會影響板片的成形性。

關鍵詞：鎂鋰合金、熱機處理、應變硬化率、成形性

Abstract

An Mg–Li based alloy containing Sc addition has been prepared by melting and solidification in a carbon steel crucible, and extruded at a billet preheating temperature of 200 ºC with an extrusion ratio of 28. Thermomechanical processing and press forming tests were performed to investigate the effect of minor addition of Sc on the mechanical properties and formability. Thermomechanical treatment, tensile tests and press forming tests were carried out to explore the variations in the strain hardening behavior and formsbility. The Mg–Li based alloy with Sc addition could be work hardened. Thermomechanical treatment could enhance the strain-hardening effect to improve the mechanical properties. Kocks–Mecking type plots were used to illustrate different stages of strain hardening of the cold rolled specimens. The results indicated that cold rolled LAZ1010Sc alloy showed stage III and stage IV strain-hardening behaviors. Press forming tests indicate that the formability of the rolled LAZ1010Sc sheet would be influenced by the orientation and deformation rate.

Keywords: Mg-Li alloy; Strain-hardening rate; Formability parameter; Forming limit diagram; Formability

1. Introduction

Alloying Mg with lithium yields a lightest structural metal of Mg−Li alloy. The Mg−Li phase diagram [1] indicates that when the Li content is between ~5.5 and 11.5 wt%, the BCC structured β phase of the Li solid

solution coexists with the HCP α phase of the Mg solid solution. As the amount of Li added to the Mg−Li alloy increases, the α phase still possesses HCP structure, but the crystal lattice axes ratio, c/a decreases such that slip between crystal planes become less difficult [2], the coexistence of the β phase makes the Mg−Li alloy possible to be cold worked. The β single phase structure could exist in Li contents greater than 11 wt%. However, the mechanical properties of Mg−Li alloys are not particularly favorable for structural applications due to its low tensile and yield strength. Various third elements have been added to the Mg−Li alloy systems to explore the effect of the addition of a third element on the mechanical properties and formability [3-5].

Strain hardening behavior is one of the important considerations in evaluating plastic deformation of materials [6], and the strain-hardening exponent is also the most important factor that influences stretchability, when stretching dominates in the forming processes [7,8]. The strain hardening behavior of cubic metals is fairly well understood and accumulation of a forest of dislocations is the dominant hardening mechanism [9,10]. Hexagonal metals present a more complex case due to their low symmetry, which restricts the number of slip systems [9], and their strong plastic anisotropy.

In the present work, an Mg–Li–Al–Zn alloy (designated as LAZ) containing about 10wt% of Li was chosen as the matrix alloy. Main emphasis was placed on investigating the effect of thermomechanical treatment on the strain-hardening behavior and formability of the LAZ alloy containing minor Sc.

2. Materials and Experimental Procedures

2.1 Alloys

The Mg–Li alloy was melted in a high-vacuum electric induction furnace under an argon atmosphere and then cast into an ingot with a cylindrical shape of 200 mm in diameter and 400 in mm height. The analyzed chemical composition of the cast alloy by use of an induction coupled plasma (ICP) and Spark Optical Emission Spectrometry (Spark-OES) apparatuses is given in Table 1. The cylindrical ingots were then extruded into a plate of 110 mm in width and 10 mm in thickness at a billet preheating temperature of 200°C.

Table 1 Chemical composition of the LAZ1010Sc alloy

Elements	Li	Al	Zn	Sc	Mg
wt%	10.41	1.02	0.46	0.01	Rem.

2.2 thermomechanical processing

The as-extruded specimen for alloy LAZ1010Sc was annealed at 300°C for 1 h followed by quenching. The annealed specimen was cold rolled with the reductions of 20, 40, 60, and 80%. Reference specimens for comparison were directly cold rolled from the extruded plate with the same reductions as used for the annealed specimens to explore the effect of annealing heat treatment on cold working.

2.3. Tensile Tests

Uniaxial tension test was carried out in the direction along the extrusion and rolling direction. The gauge length and width of the tensile specimen were 50 and 6 mm, respectively. The specimens were tested at room temperature with initial strain rates of 1.67×10^{-3} and 3.34×10^{-2} s^{-1}.

2.4 Press forming tests

The press forming tests were performed at room temperature and the punch speeds were kept constants at 6 and 30 mm/min during the tests. The sheet length for press forming test to determine the FLD was 100 mm with various width. Decreasing the width from 100 to 10 mm causes change in the state of strain from near balanced-biaxial tension through plane strain to uniaxial-tension. Two sets of samples were prepared

for press forming tests. In the first set, the length of the cut sheet was parallel to the rolling direction. In the other set, the length of the sheet was perpendicular to the rolling direction. Grid circles of diameter d_o (2.5 mm) etched on the sheets were used to measure strain levels in each test. During forming the etched circles were distorted into ellipses and/or larger circles, and these deformed grid circles were then used to measure strain levels in each case. Measurements of the major (d_1) and minor (d_2) diameters of the deformed circles after deformation were made to determine the major strains (ε_1) and the minor strains (ε_2). The major strains and the minor strains can then be expressed as:

$$\varepsilon_1 = \ln(d_1 / d_0) \quad (1)$$

$$\varepsilon_2 = \ln(d_2 / d_0) \quad (2)$$

FLDs were drawn by plotting the minor strain in abscissa and corresponding major strain in ordinate and by drawing a curve which separates the safe region from the unsafe region.

2.5 Metallographic inspection

The specimen for microscopic examination was prepared by conventional metallographic techniques. The polished specimen was etched for 1~5 sec in the etchant of 5 g picric acid, 10 ml acetic acid, 95 ml ethyl alcohol. Optical microscopy was used to examine the microstructures.

3. Results and Discussion

3.1 Analysis of the microstructure

Fig. 1 shows the as-cast structures of LAZ1010Sc alloy; the cast alloys contain both the major β–Li phase and minor α–Mg phase. The Li content of LAZ1010Sc alloy is about 10.41 wt% which is near the region of single β phase, so only few dispersed α phase particles exhibit in the microstructure, as demonstrated in Fig. 1(a), and α phase exhibits two types of morphology, one is clustered particles located in the grains and along the grain boundaries, and the other is small rod-shaped particles inside the grains, as given in Fig.1(b).

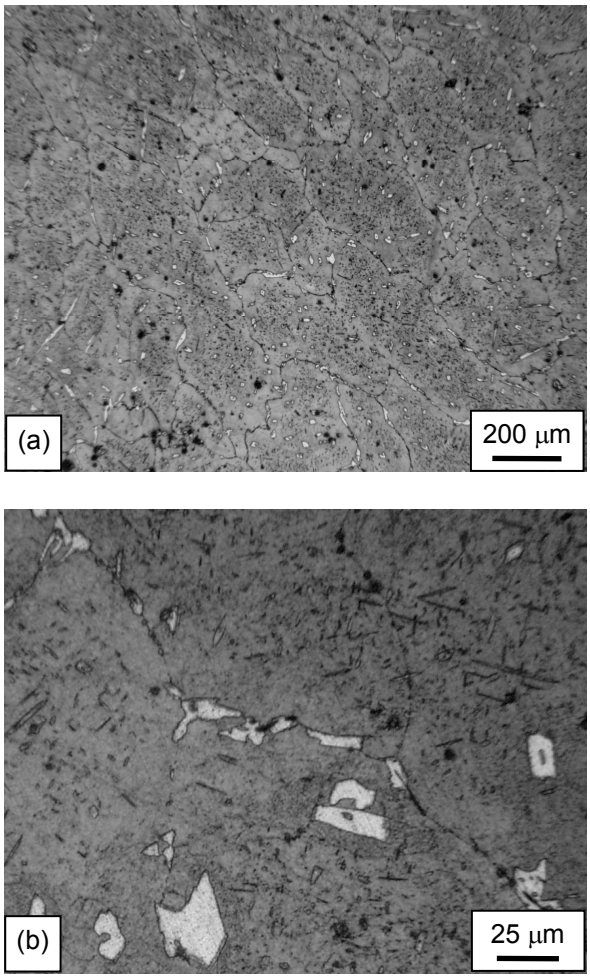

Fig.1. Optical micrographs of the as-cast microstructures. (a) LAZ1010Sc alloy, (b) LAZ1010Sc alloy on a larger scale.

Fig 2 demonstrates the as-extruded microstructure of alloy LAZ1010Sc. Fibrous structures were not observed in this study. Dynamic recrystallization should have taken place during extrusion, and some grain growth could be found in the as-extruded structure. Dynamic recrystallization of β phase was also found in the as-extruded Mg–8.7Li and Mg–8.5Li–6.4A1 alloy [11]. The rod-shaped particles still present inside the grains.

3.2 Mecahnical properties

Fig. 3 illustrates the variation in hardness with thickness reduction for the as-extruded and annealed specimens. Increase in

Table 2 Mechanical properties of the cold rolled specimens of LAZ1010Sc alloy without a prior annealing treatment

Property	Thickness reduction (%)				
	As-extruded	20	40	60	80
Yield strength (MPa)	126.7	142.3	160.4	166.1	172.4
Tensile strength (MPa)	151.9	167.0	173.0	185.0	202.2
Elongation (%)	41.1	31.7	26.7	21.3	16.1

Table 3 Mechanical properties of the cold rolled specimens of LAZ1010Sc alloy with a prior annealing treatment

Property	Thickness reduction (%)				
	As-extruded	20	40	60	80
Yield strength (MPa)	126.7	192.3	201.1	207.4	213.8
Tensile strength (MPa)	151.9	212.2	218.0	222.8	234.8
Elongation (%)	41.1	27.1	21.8	16.6	11.1

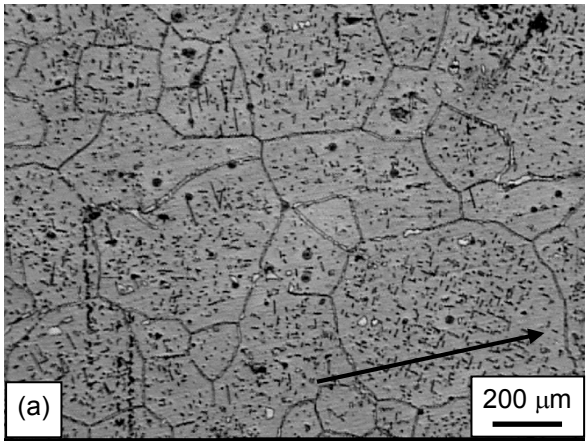

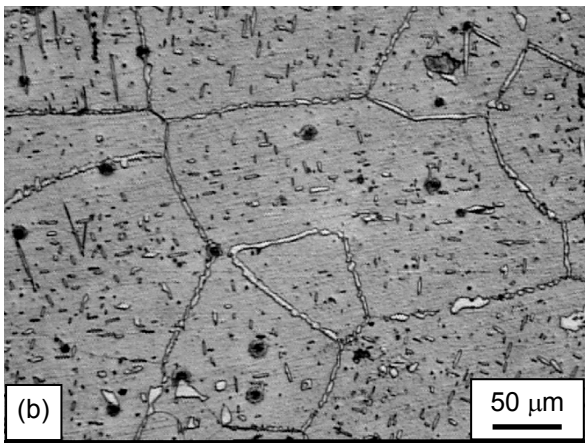

Fig.2. Micrographs of the as-extruded microstructures; the arrow indicating the extrusion direction. (a) LAZ1010Sc alloy, (b) LAZ1010Sc alloy on a larger scale.

hardness with thickness reduction indicates

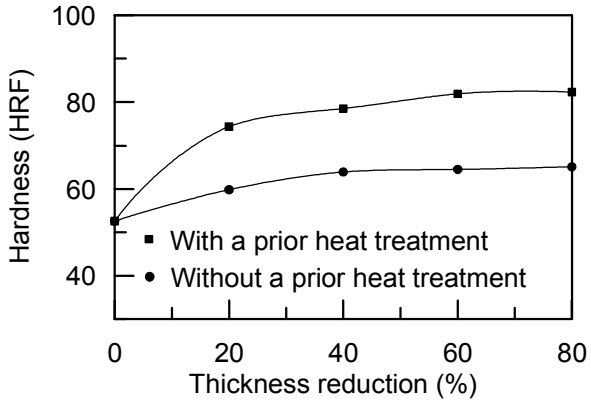

Fig. 3. Hardness variations of LAZ1010Sc alloy with different thickness reductions showing the effect of prior annealing treatment.

that LAZ1010Sc alloy could be work hardened. For the specimens with a prior annealing treatment, the strain hardening rates with reductions below 40% are higher than those of the specimens without a prior annealing treatment. Therefore, a prior annealing treatment could enhance strain hardening effect for LAZ1010Sc alloy.

Fig. 4 shows representative true stress and strain curves of the alloy tested at an initial strain rate of 1.67×10^{-3} s^{-1}. It is seen that the yield strength is higher for the higher thickness reduction, while the strain-hardening behavior is generally similar for all specimens. The mechanical properties of

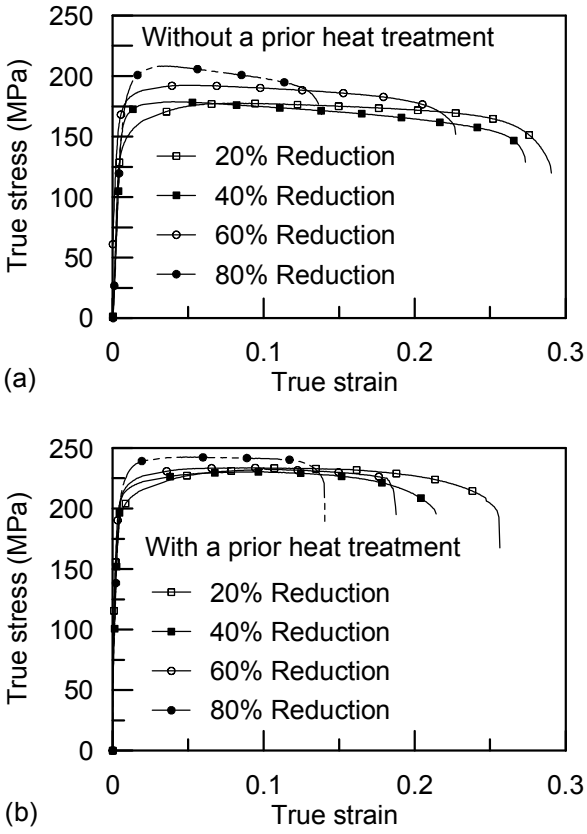

Fig. 4. Typical true stress vs. true strain curves of LAZ1010Sc alloy with various thickness reductions tested at an initial strain rate of 1.67×10-3 s-1. (a) Without a prior heat treatment, (b) With a prior heat treatment.

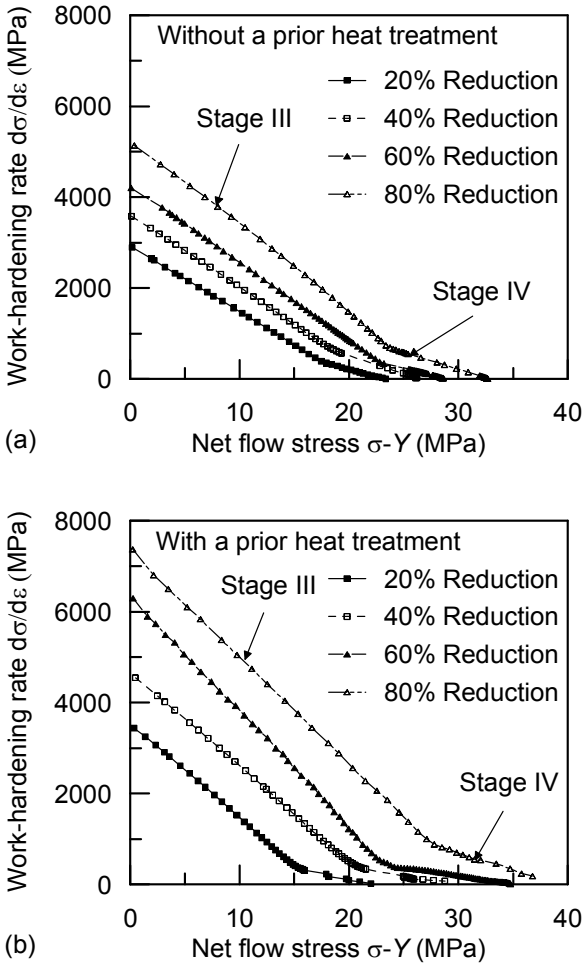

Fig. 5. Strain hardening rate (Θ) as a function of net flow stress (σ–*Y*) of LAZ1010Sc alloy tested at an initial strain rate of 1.67×10^{-3} s^{-1}. (a) Without a prior heat treatment, (b) With a prior heat treatment.

the specimens without a prior annealing treatment are listed in Table 2. Increases in tensile strength for a reduction of 80% is 33.1% for LAZ1010Sc alloy. Although the elongation decreases with increasing reduction, the LAZ1010Sc alloy still presents an elongation of 16.1% with a thickness reduction of 80%. Table 3 displays the mechanical properties of the specimens with a prior annealing treatment. Significant increases in strengths, compared to the properties of the as-extruded specimens, were found for the specimens with a prior annealing treatment. An increases in tensile strength for a reduction of 80% is 54.6% for LAZ1010Sc alloy.

3.3 Strain-hardening behavior

A Kocks–Mecking type plot of the strain-hardening behaviors of the specimens with various thickness reductions is illustrated in a plot of strain-hardening rate Θ ($d\sigma/d\varepsilon$) versus net flow stress (σ-Y), where Y is the (0.2% off-set) yield strength, during the plastic deformation at an initial strain rate of 1.67×10^{-3} s^{-1}; as shown in Fig. 5, which is derived from Fig. 4. It is evident that, for all specimens, their strain-hardening rates decrease with increasing net flow stress. Θ decreases rapidly and linearly, stage III hardening [19,20], characterized by a linear decrease in Θ, appears immediately after yielding. At higher net flow stresses, Θ becomes small and hardening stage IV [12] occurs. Specimens with a prior heat treatment show higher Θ values and higher decrease rates of Θ with net flow stress.

The strain-hardening of a material after yielding is related to the dislocation strain field interactions. Thus the Taylor dislocation contribution $\sigma_d = M\eta Gb\rho^{1/2}$ dominates the strain hardening effect; where ρ is the dislocation density, η is a constant, M is the Taylor factor, G is the shear modulus and b is the Burgers vector. Stress contribution due to dislocation density can be obtained by subtracting the yield stress from the total flow stress and can be written as $\rho^{1/2} \propto \sigma_d = \sigma\text{-}Y$ [13]. Then the applied stress necessary to deform a material is proportional to the dislocation density inside the material resulting in a high and nearly constant strain-hardening rate (i.e. stage II linear hardening effect). However, the cold worked specimens in the present study do not exhibit any stage II linear hardening behavior, and their stage III with a decreasing Θ occurs immediately after yielding, as shown in Fig. 5. The dominant slip system in Mg and Mg alloys at room temperature is the basal one. The activity of non-basal slip systems plays an important role in softening. Addition of Li may result in higher activity of non-basal slip [14]. Screw component of **a** (basal) dislocations in the basal planes may move on the prism planes [15]. Therefore, the free path of dislocations increases and strain hardening rate decreases. This could be the reason for the occurrence of stage III strain hardening after yielding in the LAZ1010 alloy due to easy cross-slip.

As stage III appears to approach a saturation level, the new stage IV gets involved when the hardening rate Θ has dropped to a particular low level. Stage IV has been found in some polycrystalline metals [16,17]. Sevillano et al. [18] postulated that Θ decreased continuously in stage IV and that it was terminated by damage accumulation, eventually leading, at the end of stage IV, to failure and a corresponding drop of Θ. Rollett et al. [19] proposed that the hardening rate in stage IV was governed by debris accumulation in the cell walls. While in the major part of stage III the net rate of dislocation accumulation was rather high as compared to that of debris accumulation, the latter became dominant at the end of stage III in the new stage IV.

Table 4 Formability parameters of the LAZ1010Sc alloy sheet

Property	1.67×10^{-3} s^{-1}	3.34×10^{-2} s^{-1}
r_{RD}	1.876	1.237
r_{45}	2.090	1.539
r_{TD}	2.872	2.248
Average ($\bar{r}$)	2.232	1.641
Δr	0.284	0.204

3.4. Formability parameters

The formability parameters at initial strain rates of 1.67×10^{-3} s^{-1} and 3.34×10^{-4} s^{-1} determined by experiments are tabulated in Table 4. A metal sheet with a higher value of $\bar{r}$ (normal anisotropy) could promote good deep-drawability [20], and a higher Δr value (planar anisotropy) would increase the tendency of ear formation during drawing operation. Both the $\bar{r}$ value and its Δr value are highly dependent upon texture, or preferred orientation [21]. Higher r value was observed in the TD.

The r values at room temperature and at a strain rate of 1.67×10^{-3} s^{-1} are 1.876 and 2.872 in the RD and TD samples, respectively. In the study demonstrated by Chino et al. [22], a rolled sheet with a low r value corresponds to enhancement of thickness direction strain. Therefore, the stretchability of the RD sample should be better than that of the TD sample. A higher n value was also observed in the RD. As reported in the literatures [20,23], when stretching predominates in the forming processes, n is the most important factor that influences stretchability and the metals having a high n value represent greater stretchability. The RD sample shows not only a lower r value but also a higher n value indicating that the stretchability of the RD sample should be better than that of the TD sample at room temperature and at a strain rate of 1.67×10^{-3} s^{-1}. Although a lower r value could improve the stretchability, it would exhibit lower deep drawability.

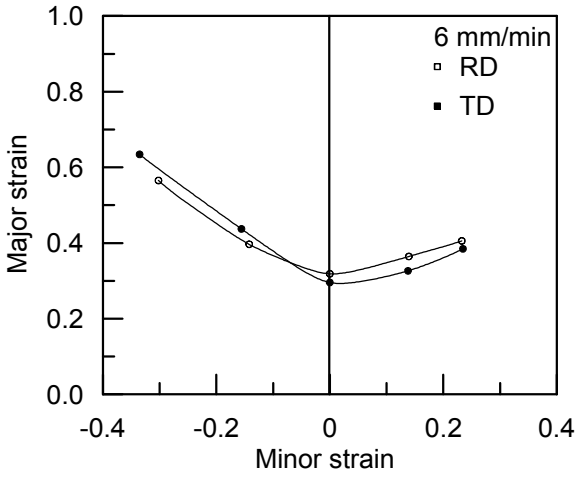

Fig. 6. Forming limit diagrams of the LAZ1010Sc alloy sheets at a punch speed of 6 mm/min. RD: The rolling direction of the test piece is parallel to the major strain. TD: The rolling direction of the test piece is perpendicular to the major strain.

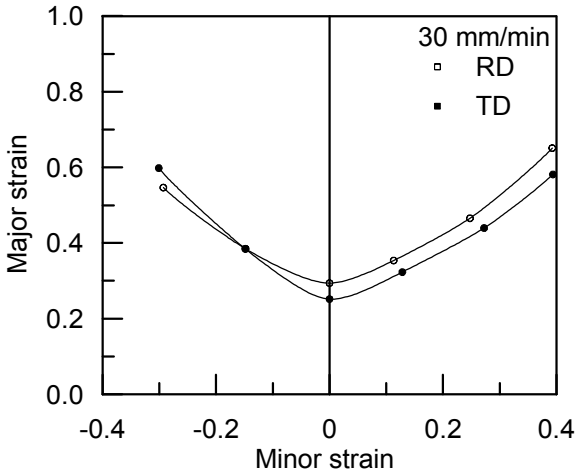

Fig. 7. Forming limit diagrams of the LAZ1010Sc alloy sheets at a punch speed of 30 mm/min. RD: The rolling direction of the test piece is parallel to the major strain. TD: The rolling direction of the test piece is perpendicular to the major strain.

Because the stress state of stretch forming is biaxial tension, and the stress state of deep drawing approaches pure shear in the flange and the plane strain tension in cup wall. The planar anisotropy Δr is estimated to have a large positive value of 0.284. A large value of Δr indicates the high earing tendency of the alloy during drawing operation at room temperature.

Similar results were also observed for the sheets tested at a higher initial strain rate of 3.34×10^{-2} s^{-1}. As the strain rate increases the average n value increases and $\bar{r}$ value decreases indicating that the stretchability could be improved by increasing the forming rate. Decrease in elongation and $\bar{r}$ value reveal that increase in strain rate at room temperature is unfavorable to the drawability.

3.5. Forming limit diagrams

Fracture limit curves plotted as the forming limit diagrams of the LAZ1010Sc alloy sheet at a punch speed of 6 mm/min from the experimental results are displayed in Fig. 6. The RD designation in Fig.6 means that the rolling direction of the test piece is parallel to the major strain and the TD means that the rolling direction is perpendicular to the major strain. In the biaxial tensile region, the RD samples show higher major strains than those of the TD samples in good agreement with the RD samples having higher n values and low r-values at both temperatures. The TD samples show high formability under uniaxial tensile stress compared with the RD samples, in agreement with the TD having higher r-values.

The forming limit diagrams tested at a punch speed of 30 mm/min are illustrated in Fig. 7. In the biaxial tension region, some increases in limiting strains at room temperature were observed due to a decrease in $\bar{r}$ value when compared with the sample deformed at a lower punch speed of 6 mm/min. However, in the uniaxial tension region, decreases in limiting strains have taken place resulting from a decrease in $\bar{r}$ value at a higher punch speed, in agreement with forming parameters obtained from tensile tests. Theses results indicates the stretchability of the LAZ1010Sc sheet could not be significantly improved at room temperature by increasing the deformation rate.

4. Conclusions

The effects of thermal and mechanical treatments on the strain-hardening behaviors and formability of an Mg–Li–based alloy containing minor addition of Sc were investigated in this study. The LAZ1010Sc alloy sheets did not exhibit any stage II linear hardening behavior, and their stage III with a decreasing strain-hardening rate occurred immediately after yielding. The activation of non-basal slip and cross-slip should be the reason to suppress the stage II hardening behavior.

Increase in the deformation rate, which would increase the n value and decrease r-value, could improve the stretchability; on the contrary, decrease in r-value revealed that increase in deformation rate would not favor the drawability. Higher n values and lower r-values were observed in the RD samples. Therefore, the RD samples exhibited higher stretchability and the TD samples revealed higher drawability. At a higher punch speed of 30 mm/min during press forming, the decrease in $\bar{r}$ value and the increase in average n value, when compared with the samples deformed at a lower punch speed of 6 mm/min, resulted in an enhanced stretchability.

Acknowledgments

This work was conducted through grants from National Science Council under the contract NSC 96-2212-E-216-012.

References

[1] A.A. Nayeb-Hashemi, J.B. Clark, A.D. Pelton, Bulletin of Alloy and Phase Diagrams 5 (1984) 365–374.
[2] F.H. Herbstein, B.L. Averbach, Acta Metall. 4 (1956) 407–413.
[3] J.Y. Wang, W. P. Hong, P.C. Hsu, C.C. Hsu, S. Lee, Mater. Sci. Forum 419-422 (2003) 165–170.
[4] A. Yamamoto, T. Ashida, Y. Kouta, K.B. Kim, S. Fukumoto, H. Tsubakino, Mater. Trans. 44 (2003) 619–624.
[5] F. von Buch, J. Lietzau, B.L. Mordike, A. Pischb, R. Schmid-Fetzer, Mater. Sci. Eng. A263 (1999) 1–7.
[6] X.H. Chen, L. Lu, Scripta Mater. 57 (2007) 133–136.
[7] D. Ravi Kumar, K. Swaminathan, Mater. Sci. Technol. 15 (1999) 1241–1252.
[8] Z. Marciniak, K. Kuczynski, T. Pokora, Int. J. Mech. Sci. 15 (1973) 789–805.
[9] U.F. Kocks, H. Mecking, Prog. Mater. Sci. 48 (2003) 171–273.
[10] H. Mecking, U.F. Kocks, Acta Metall. 29 (1981) 1865–1875.
[11] A. Sanschagrin, R. Tremblay, R. Angers, D. Dubé, Mater. Sci. Eng. A220 (1996) 69-77.
[12] U.F. Kocks, H. Mecking, Prog. Mater. Sci. 48 (2003) 171–273.
[13] J.A. del Valle, F. Carreno, O.A. Ruano, Acta Mater. 54 (2006) 4247–4259.
[14] S. Kamado, Y. Kojima, Metall. Sci. Technol. 16 (1998) 45–54.
[15] Z. Trojanová, Z. Drozd, P. Lukáč, F. Chmelík, Mater. Sci. Eng. A410–411 (2005) 148–151.
[16] N. Afrin, D.L. Chen, X. Cao, M. Jahazi, Scripta Mater. 57 (2007) 1004–1007.
[17] O. Nijs, B. Holmedal, J. Friis, E. Nes, Mater. Sci. Eng. A483–484 (2008) 51–53.
[18] J.G. Sevillano, P. van Houtte, E. Aernoudt, Prog. Mater. Sci. 25 (1980) 69–134.
[19] A.D. Rollett, Ph.D. Thesis, Drexel University, Philadelphia, 1988.
[20] D. Ravi Kumar, A. Sen, K. Swaminathan, J. Mater. Sci. Letters 13 (1994) 971–973.
[21] W.F. Hosford, Mater. Sci. Eng. A 257 (1998) 1–8.
[22] Y. Chino, K. Sassa, A. Kamiya, M. Mabuchi, Mater. Sci. Eng. A 441 (2006) 349–356.
[23] Z. Marciniak, K. Kuczynski, T. Pokora, Int. J. Mech. Sci. 15 (1973) 789–805.

計畫成果自評

本研究依據原計畫目標完成含鈧超輕鎂鋰合金之性質研究，完成之工作項目如下所述：

(1) 含鈧鎂鋰合金的熔煉
(2) 含鈧鎂鋰合金厚板擠製
(3) 含鈧鎂鋰合金精密薄板軋延
(4) 含鈧鎂鋰合金金相分析
(5) 含鈧鎂鋰合金熱機處理
(6) 含鈧鎂鋰合金加工硬化行為探討
(7) 含鈧鎂鋰合金成形性分析

本計畫完成了含鈧鎂鋰合金薄板壓延製作技術及性質分析。就研究成果之學術價值而言，適合在國外SCI等級以上之學術期刊發表。研究成果已撰寫論文一篇，以論文題目為"Strain-hardening behavior and formability of Mg-Li-Al-Zn alloy with minor Sc addition"投寄國際期刊Materials Science and Engineering A。

本研究計畫之主要發現，而且也未在其它學術期刊所發表之重要成果包括下列所述之幾項：

1. LAZ1010Sc 合金具有應變硬化的效果，熱機處理會影響應變硬化的效應。冷軋延前，經退火熱處理，其硬度較未經過熱處理提升許多，但其硬度趨勢與未經過熱處理之合金類似，顯示適當之熱處理有助於提升冷加工後之硬度。
2. 以 Kocks–Mecking 的應變硬化率分析結果顯示，含鈧 LAZ1010 合金並未顯示第 II 階段的線性硬化行為；在降伏點之後，立即出現第三階段的硬化行為。這主要是添加鋰元素後，促進了非基面滑移及交叉滑移，因而抑制了第 II 階段應變硬化的現象。
3. LAZ1010Sc 合金在室溫下，隨變形應變速率的提升，n 值及 $\bar{r}$ 值均有增加的趨勢，而 Δr 值則隨之下降；意即 LAZ1010Sc 合金在室溫下提高其應變速率，可以增加對板材的引張性(Stretchability)。若在引張變形為主的成形製程中，提高變形速率，生產速度可大幅的增加，且應對於板材之成形性有相當大的助益。
4. LAZ1010Sc 合金的成形極限圖顯示，在較慢的變形速率下，可以改善板片的深抽性(Drawability)。因此，在深抽的成形製程中，應採用較慢的成形速率，以增加其深抽性。
5. LAZ1010Sc 之成形不但受到變形速率的影響，板片製作所產生的軋延方向也會影響板片的成形性。軋延方向若與主要變形方向平行，可以增加板片的引張性，有利於雙軸向的拉伸變形。反之，主要變形方向若垂直於板片軋延方向，則可以增加板片的深抽性。

行政院國家科學委員會補助國內專家學者出席國際學術會議報告

98 年 3 月 24 日

附件三

報告人姓名	吳泓瑜	服務機構及職稱	中華大學機械系教授
時間 會議 地點	980318~980320 國際工程師協會學術研討會 香港	本會核定 補助文號	計畫編號 NSC 2221-E-216-010
會議名稱	(中文)2009 年工程師及電腦科學家國際學術研討會 (英文) International MultiConference of Engineers and Computer Scientists IMECS 2009		
發表論文題目	(中文)AZ31B 細晶鎂板快速氣壓成形之變形特性 (英文) Deformation characteristics of fine-grained magnesium alloy AZ31B thin sheet during fast gas blow forming		

報告內容應包括下列各項：

一、參加會議經過

1. 此項國際學術研討會於香港的九龍富豪酒店舉辦，為期三天。
2. 三月十八日 9:00~17:00 論文發表，共發表 Workshop-based work systems design 等 23 篇論文。
3. 三月十九日 09:00~17:30 論文發表，共發表 Improvement of scheduling efficiency using heuristic methods and simulation technique in electronic assemblies industry production 等 23 篇論文。
4. 三月二十日 09:00~17:00 論文發表，共發表 What decision factors will affect design for base of the pyramid (DfBoP)? An experience research based on case study from IDE/TU 等 21 篇論文。
5. 三月十九日晚於九龍富豪酒店三樓的凡爾賽廳舉辦晚宴，提供與會專家學者之交流機會。

二、與會心得

本項學術研討會由國際工程師協會(International Association of Engineers)主辦。國際工程師協會為非營利性的國際協會，每年固定於英國倫敦，美國舊金山及香港等三地舉辦三項國際學術研討會。世界工程師研討會(The World Congress on Engineer, WCE)每年七月於英國倫敦帝國大學(Imperial College)舉辦。世界工程及資訊科學研討會(The World Congress on Engineering and Computer Science, WCECS)十月於美國加州柏克萊舉行。工程師及資訊科學國際多項研討會(The International MultiConference of Engineers and Computer Scientists, IMECS)則於三月於香港舉辦。研討會論文的審查非常嚴謹，歷年來的統計顯示，論文的接受率約在 57%左右。IMECS 2009 國際學術研討會共包括 13 項會議主題 Artificial Intelligence and Applications (ICAIA)、Bioinformatics (ICB)、Control and Automation (ICCA)、Computer Science (ICCS)、Communication Systems and Applications (ICCSA)、Data Mining and Applications (ICDMA)、Electrical Engineering (ICEE)、Imaging Engineering (ICIE)、Industrial Engineering (ICINDE)、Internet Computing and Web Services (ICICWS)、Operations Research

(ICOR)、Scientific Computing (ICSC)、Software Engineering (ICSE)等。本人所參加的為 ICINDE 項主題,此項主題所發表之論文共計口頭報告 67 篇,張貼論文發表 7 篇,論文內容豐富。參加此項會議,可以充分了解現階段工業的發展趨勢,以及未來的應用方向,有助於國內未來學術研究發展及應用的參考。此項會議就本人而言,可謂獲益良多。會議中並與相關領域的國外學者進行交流,提高我國相關研究之國際知名度。

三、考察參觀活動(無是項活動者省略)

無

四、建議

應鼓勵國內教師多參與國際性學術研討會,除了促進國際學術交流外,也可以提升國內學者的國際觀,增進研究績效。

五、攜回資料名稱及內容

1. The International MultiConference of Engineers and Computer Scientists 2009 論文集紙本
2. The International MultiConference of Engineers and Computer Scientists 2009 論文及光碟片兩片
3. The International MultiConference of Engineers and Computer Scientists 2009 Program Schedule and Session Details
4. International Association of Engineers 會訊

六、其他

Deformation Characteristics of Fine-grained Magnesium Alloy AZ31B Thin Sheet during Fast Gas Blow Forming

Pin-hou Sun, Horng-yu Wu, Shyong Lee, Chui-hung Chiu

***Abstract*—A series of experiments were performed by use of stepwise pressurization profiles for gas blow forming of an Mg alloy with a male die. Decreasing the forming time for gas blow forming of a commercially available fine-grained Mg alloy AZ31B thin sheet with a thickness of 0.6 mm has been studied in the present work. The results indicated that it was feasible to form a shallow rectangular pan with a height of 10 mm in less than 320 sec. The distribution of thickness along the transverse cross section of the formed pan was confirmed by the results as being sensitive to the pressurization profiles. Grain growth was not a serious problem for forming at a temperature of 370°C. Grain size increased from about 5.1 μm to a maximum size of about 7.1 μm. The maximum cavity volume fraction in the formed pan was about 1.1% for two different pressurization profiles.**

***Index Terms*—AZ31B Mg alloy, Gas blow forming, Pressurization profile**

I. Introduction

Magnesium is the lightest metal that can be used in structural applications when alloyed with other elements. Research on Mg alloy focusing on mechanical properties has become very active in the past decade [1]–[3]. In recent years, die casting of Mg alloys has been developed for electronic appliances and automotive components [4], [5]. However, casting is not an ideal process in manufacturing thin-walled Mg components due to its low yield and low good rates. A potential solution would be to turn to the sheet forming processes.

In light of hexagonal close-packed (HCP) structure, Mg and its alloys have crucial drawback of poor formability, especially at room temperature, than aluminum and its alloys. Therefore, sheet metal forming operation for Mg alloy would be generally carried out at temperatures up to 300 °C [6]. In order to improve the formability of the Mg alloy thin sheet, the fine-grained (less than 10 μm) AZ31B Mg alloy has been developed and is commercially available. Components using the fine-grained AZ31B alloy sheet could be manufactured either by press forming or superpplastic gas blow forming process. Fine-grained AZ31B alloy requires careful process control to maintain the desired constant strain rate during superplastic forming. The strain rates are typically very low compared with most metal forming processes. A significant problem in commercial applications of superplastic forming with AZ31B alloy is the low forming rates (10^{-3}-10^{-4} s^{-1}), which is undesirable in a manufacturing process for mass production. In order to meet the need for industrial applications, it is necessary to increase the forming rate during gas blow forming.

The present work has explored the deformation characteristics of a commercial grade fine-grained AZ31B alloy during gas blow forming by use of rapid pressurizing profiles with the intention of reducing forming time. Gas pressure forming was performed to deform the sheet into a male die cavity to form a rectangular shaped pan. Backpressure and lubricant were not used during forming. Effects of pressurization profiles on the formability were studied. Experimental results were quantitatively analyzed and the results were presented.

II. Materials and Experimental Procedure

POSCO Company, Korea, provided the Mg alloy AZ31B-O thin sheet with a thickness of 0.6 mm used in this work. The analyzed chemical composition was (wt-%) Mg-3.01Al-0.98Zn-0.32Mn. The average grain size was about 5.1 μm before forming. The optical image of the microstructure of sheet is presented in Fig. 1. The sheet was formed into a rectangular shaped male die cavity by compressed gas. The dimensions of the formed rectangular pan were 70 mm (length) × 40 mm (width) × 10 mm (height); as shown in Fig.2. Gas blow forming was carried out at a lower die temperature of 370°C and an upper die temperature of 240°C according to the pressure-time profiles shown in Fig. 3. The terms PT320 and PT240 used in the present paper refer to the pressurization profiles for the forming periods of 320 and 240 sec, respectively. The pressurization profiles used in this work did not result in constant strain rates as the deformation proceeded; the strain rate changed with time

Manuscript received December 15, 2008. This work was supported by the National Science Council under the contract No. NSC 97-2221-E-216-010 and Chung-hua University under the contract No. CHU NSC 97-2221-E-216-010.

P. H. Sun is with the Department of Mechanical Engineering, National Central University, Chungli, Taiwan 320 ROC (e-mail: 963403030@cc.ncu.edu.tw).

H. Y. Wu is with the Department of Mechanical Engineering, Chung-hua University, Hsinchu, Taiwan 300 ROC (phone: 3-5186493; fax: 3-5186521; e-mail: ncuwu@chu.edu.tw).

S. Lee is with the Department of Mechanical Engineering, National Central University, Chungli, Taiwan 320 ROC (e-mail: shyong@cc.ncu.edu.tw).

C. H. Chiu is with the Materials and Chemical Research Laboratories, Industrial Technology Research Institute, Chutung, Taiwan 310 ROC (e-mail: davy@itri.org.tw).

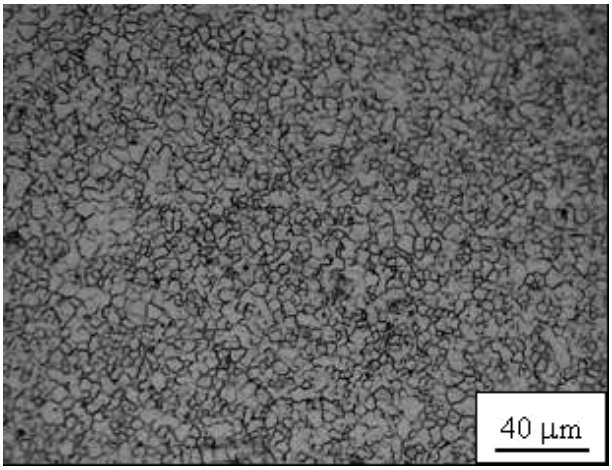

Fig. 1. Optical image of the microstructure of the fine-grained AZ31B Mg alloy.

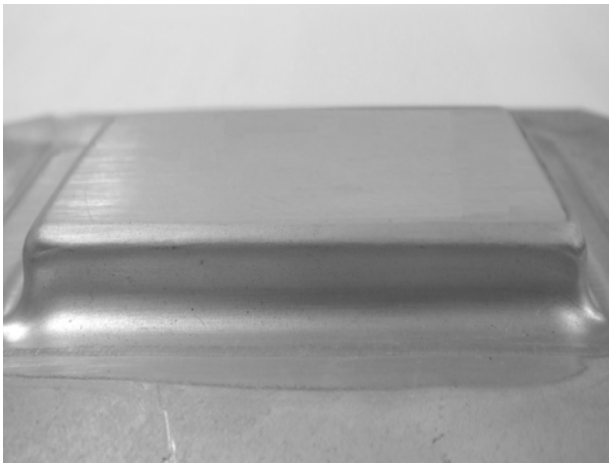

Fig. 2. Male die formed rectangular pan using fast gas blow forming.

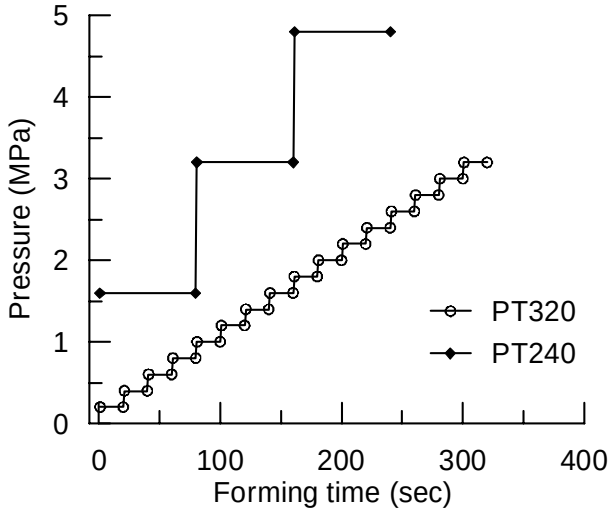

Fig. 3. Pressure-time profiles developed for fast gas blow forming.

during forming. Several interrupted tests were performed to deform the sheets to various degrees for each pressurization profile, the test piece could then be utilized to evaluate the evolution of deformation during forming. In order to obtain the fundamental information on the characteristics of a male die forming of Mg alloy AZ31B, lubricant and backpressure were not used in this study.

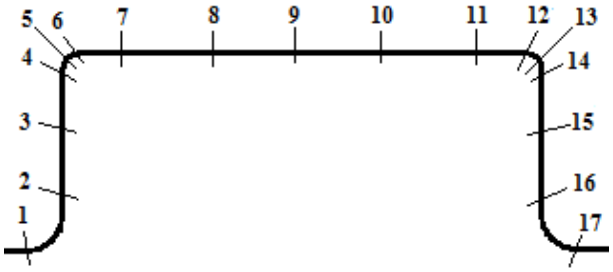

Fig. 4. The corresponding positions at which thickness, grain size and cavity volume fraction were measured.

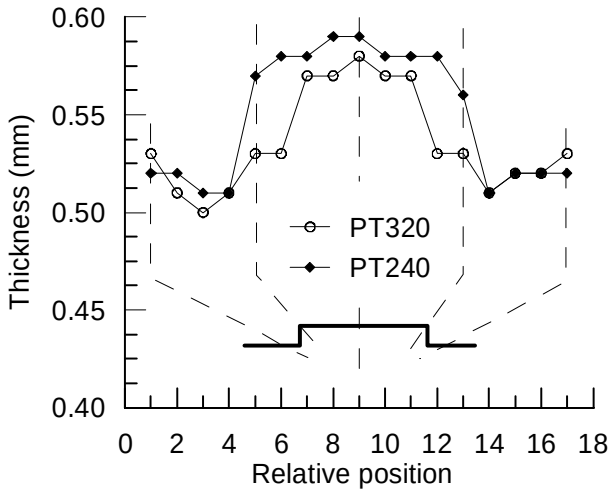

Fig. 5. Thickness distribution of the completely formed rectangular pan along the transverse cross section forming at two different pressurization profiles.

Optical microscopy was used to inspect cavitation of the test piece. The specimens for metallographic examination were mechanically polished and then slightly etched to remove smeared metal covering the cavities. Cavity volume fractions were measured by computer imaging equipment and calculated by using IMAGE-J software. The optical image was first converted into a binary video image. The number of pixels in the cavity (black area) were counted and divided by the total number of pixels in the image to obtained cavity volume fraction. Fig. 4 shows the corresponding positions at which thickness, grain size and cavity volume fraction of the formed pans were measured.

III. RESULTS AND DISCUSSION

A. Thickness Distribution

Fig. 5 depicts the thickness distribution of the completely formed rectangular pan along the transverse cross section at two different pressurization profiles. The thinnest region does not locate at the upper corner for a male die forming. The thinnest region falls at the location near the lower corner on the side wall. The thinnest thickness values are 0.51 and 0.50 mm for forming at pressurization profiles of PT240 and PT320, respectively. For forming without lubrication, the interfacial friction is large, when the sheet makes contact with the die surface, the deformation in that contact area is

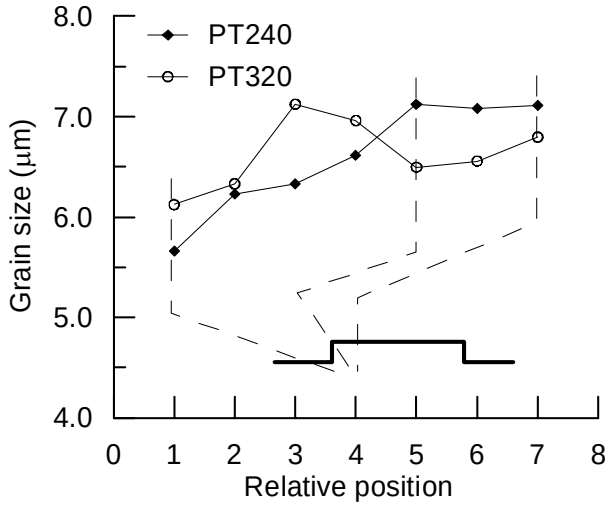

Fig. 6. Grain size distribution along the transverse cross section of the completely formed rectangular pan for forming at two different pressurization profiles.

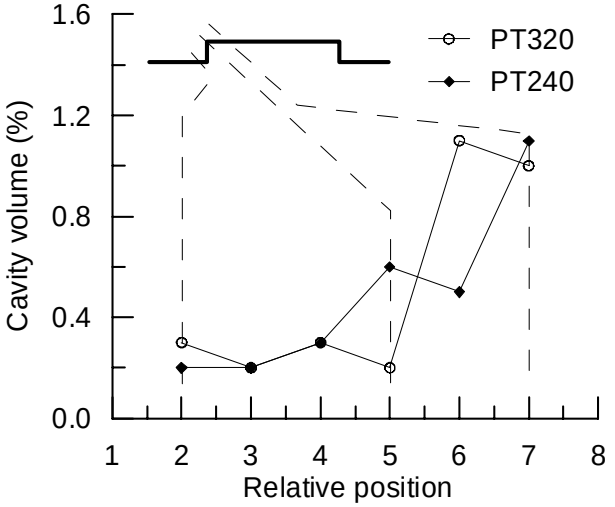

Fig. 7. Cavity volume fraction distribution along the transverse direction of the completely formed pan for forming at two different pressurization profiles.

restricted, and thinning is localized in the non-contact areas resulting in a greater degree of thinning. Major thinning effect takes place at the non-contact region of the sheet in the later stage of forming, therefore, more significant thinning was observed on the side wall region.

Thickness values on the top plane of the formed pans are about 0.58-0.59 mm and 0.57-0.58 mm for forming at pressurization profiles of PT240 and PT320, respectively. For fast gas blow forming, the imposed external pressure has a significant effect on the interfacial friction between deformed sheet and the die surface. The imposed pressures for forming at a pressurization of PT240 are much greater than those of PT320, a higher imposed pressurization profile results in a higher interfacial friction to reduce the thinning effect on the top plane of the formed pan in a male die forming.

B. Grain Size Distribution

A plot of the distribution of grain size is given in Fig. 6. It indicates that grain growth did occur during forming. Different distributions of grain size were observed for forming at different pressurization profiles. Grain growth should be related to the amount of deformation and temperature in the deformed sheet. In this study, the upper die temperature is lower than that of lower die. As the sheet is loaded, the sheet sits on the top surface of the lower male die and is heated up by the lower die. At the time when the dies are closed, the periphery of the sheet will be cooled down due to a lower upper die temperature. Therefore, a temperature gradient will exist during forming. Grain growth in the side wall region should be resulted from strain-induced grain growth due to a higher deformation in the side wall with a lower temperature. The grain growth observed in the top plane of the formed pan should be the result caused by the static grain growth due to a higher temperature in this region. The thinning effect in the top plane of the formed pan is small than that in the side wall, however, the grain size in the top plane region is greater than that in the side wall region. This result reveals that static grain growth is the major factor to cause grain growth during fast gas blow forming.

Fig. 6 also shows that the locations with maximum grain size are different for forming at different pressurization profiles. The maximum grain size locates at position 3 which is the thinnest position of the pan formed at a pressurization profile of PT320. The forming time for forming at a pressurization profile of PT320 is longer than that of PT240 reducing the temperature gradient across the sheet during forming. The temperature at position 3 for forming at a pressurization profile of PT320 should be higher than that for forming at a pressurization of PT240, both static and strain-induced grain growth should have taken place at position 3 for forming at a pressurization of PT320 resulting in a larger grain size.

C. Cavity Distribution

Fig. 7 displays the distribution of cavity volume fraction of the formed pan. It shows that the distributions of cavity volume fraction are not much different for forming at two different pressurization profiles. The maximum cavity volume fraction is about 1.1% for both pressurization profiles, indicating that cavitation is not a serious problem in this study. Cavitation in the fine-grained alloys during gas blow forming should be related to the strain rate, stress state, strain and grain size [7]–[9]. In this study, no obvious relationship between cavity level and the parameters mentioned above was observed. In general, the cavity level increases with grain size. A more detailed study should be performed to clarify the cavitation behavior of the fine-grained AZ31B Mg alloy during fast gas blow forming using a male die.

D. Thickness Evolution during Forming

Fig. 8 depicts the evolution of thickness at different locations of the deformed sheet with forming time at two different pressurization profiles. For forming at a pressurization profile of PT320, the thickness at position 7 in the top plane decreases with increasing forming time, reaches a thickness of about 0.57 mm at a forming time of around 150 sec and then remains constant, as shown in Fig 8(a). Similar result was also observed at position 2 near the

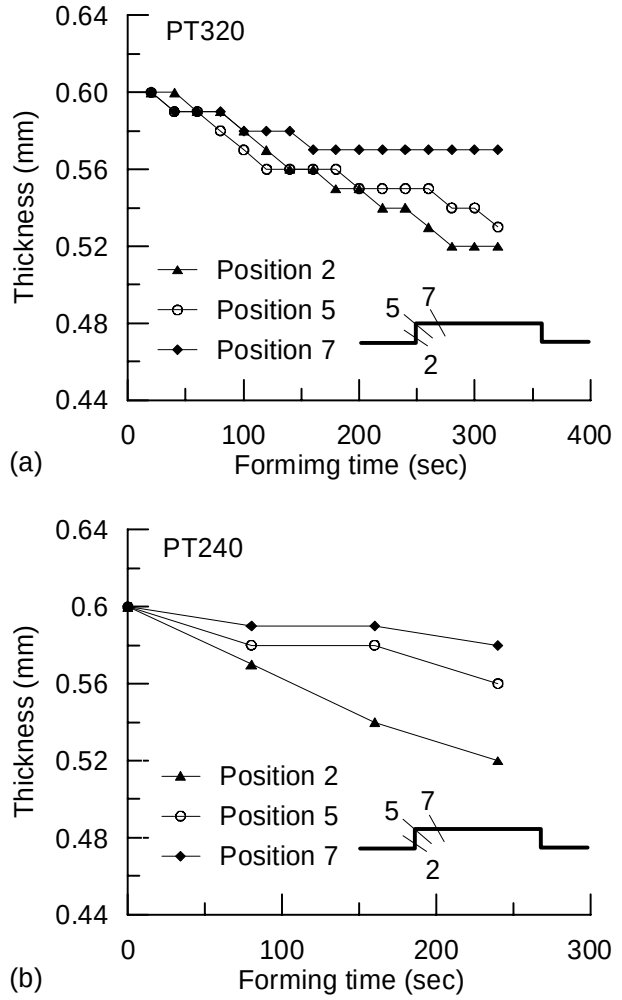

Fig. 8. Thickness evolution during forming for forming at two different pressurization profiles. (a) PT320, (b) PT240.

bottom corner on the side wall in the later stage of forming. Although constant thickness at position 5 (upper corner) took place in the middle stages of forming, no constant thickness was observed at the end of forming.

For forming at a pressurization profile of PT240, evolution of thickness with forming time presents a different trend, as shown in Fig. 8(b). The deformed sheet does not reach constant thickness towards the end of forming. For a male die forming, the sheet is placed on the top surface of the lower die. The interfacial friction would restrict the metal flow in the top plane region of the pan, and major deformation takes place in the side wall region. A pressurization profile of PT240 imposes a larger pressure which has the ability to pull the metal to flow from the top plane towards the side wall in the later stage of forming. Therefore, no constant thickness is reached in the later stage of forming.

IV. CONCLUSIONS

A male die forming of a fine-grained Mg alloy AZ31B through usage of stepwise pressurization profiles was undertaken in this present study. Using non-optimum pressurization profiles allowed the fast gas blow forming to be achieved and significantly reduced the forming time. A rectangular shaped pan with a length of 70 mm, a width of 40 mm and a height of 10 mm could be successfully formed in less than 320 sec. Interfacial friction between the lower die surface and the deformed sheet restricted the metal flow in the top plane of the formed pan, major thinning effect took place in the side wall region. The distributions of cavity volume fraction were not much different for forming at two different pressurization profiles used in this study. The maximum cavity volume fraction was only about 1.1% for both pressurization profiles. Fast gas blow forming of Mg alloy AZ31B showed its potential for future applications.

REFERENCES

[1] G. S. Cole and A. M. Sherman. (1995, July). Light weight materials for automotive applications. *Mater. Charact. 35(1).* pp. 3–9.

[2] Y. Kojima. (2991, July). Project of platform science and technology for advanced magnesium alloys. *Mater. Trans. 42(7).* pp. 1154–1159.

[3] H. Haferkamp, R. Boehm, U. Holzkamp, C. Jaschik, V. Kaese, and M. Niemeyer. (2001, July). Alloy development, processing and applications in magnesium lithium alloys. *Mater. Trans. 42(7).* pp. 1160–1166.

[4] J. A. Carpenter, J. Jackman, N. Li, R. J. Osborne, B. R. Powell, and P. Sklad. (2007, May). Automotive Mg research and development in North America. *Mater. Sci. Forum 546-549.* pp. 11–24.

[5] Y. Kojima and S. Kamado. (2005, July). Fundamental magnesium researches in Japan. *Mater. Sci. Forum 488-489.* pp. 9–16.

[6] A. Mwembela, E. B. Konopleva, and H. J. McQueen. (1997, December). Microstructural development in Mg alloy AZ31 during hot working. Scripta Mater. 37(11). pp. 1789–1795.

[7] J. Pilling and R. Ridley. (1986, April). Effect of hydrostatic pressure on cavitation in superplastic aluminum alloys. *Acta Metall. 34(4).* pp. 669–679.

[8] J. Pilling and N. Ridley, *Superplasticity in Crystalline Solids.* London: The Institute of Metals. 1989, pp. 102–158.

[9] N. Ridley. *Superplasticity.* AGARD Lecture Series No. 154. Neuilly Sur Seine, France: Advisory Group for Aerospace Research and Development. 1987, pp. 4.1–4.14.